Strong UnderIce Heating of Central Asian Shallow Lakes

Huo, Puzhen; Lu, Peng; Leppäranta, Matti Juhani; Kirillin, Georgiy; Cheng, Bin ...

2025-07-28
John Wiley and Sons Inc.
http://hdl.handle.net/10138/602542
Huo, P, Lu, P, Leppäranta, M J, Kirillin, G, Cheng, B, Xie, F & Li, Z 2025, 'Strong Under Ice Heating of Central Asian Shallow Lakes', Geophysical Research Letters, vol. 52, no. 14, e2024GL114501. https://doi.org/10.1029/2024gl114501

AGU ADVANCING EARTH AND SPACE SCIENCES

Geophysical Research Letters

RESEARCH LETTER
10.1029/2024GL114501

Strong Under-Ice Heating of Central Asian Shallow Lakes

Puzhen Huo[1], Peng Lu[1], Matti Leppäranta[2], Georgiy Kirillin[3], Bin Cheng[4], Fei Xie[1], and Zhijun Li[1]

[1]State Key Laboratory of Coastal and Offshore Engineering, Dalian University of Technology, Dalian, China, [2]University of Helsinki, Helsinki, Finland, [3]Department of Ecohydrology, Leibniz-Institute of Freshwater Ecology and Inland Fisheries (IGB), Berlin, Germany, [4]Finnish Meteorological Institute, Helsinki, Finland

Key Points:

- First, the ice season of Lake Ulansu, a shallow Central Asian lake, is monitored via a floating remote observation system
- Owing to salinity stratification, the water temperature remained unusually warm for more than 90% of the ice season
- Approximately 82% of the solar radiation absorbed by the water column returned to the ice base

Supporting Information:

Supporting Information may be found in the online version of this article.

Correspondence to:

P. Lu,
lupeng@dlut.edu.cn

Citation:

Huo, P., Lu, P., Leppäranta, M., Kirillin, G., Cheng, B., Xie, F., & Li, Z. (2025). Strong under-ice heating of Central Asian shallow lakes. *Geophysical Research Letters*, *52*, e2024GL114501. https://doi.org/10.1029/2024GL114501

Received 29 DEC 2024
Accepted 3 JUL 2025

Author Contributions:

Conceptualization: Puzhen Huo, Peng Lu, Matti Leppäranta
Formal analysis: Georgiy Kirillin, Bin Cheng, Fei Xie, Zhijun Li
Funding acquisition: Peng Lu, Georgiy Kirillin, Zhijun Li
Investigation: Puzhen Huo
Supervision: Peng Lu, Matti Leppäranta
Validation: Georgiy Kirillin, Bin Cheng, Fei Xie, Zhijun Li
Visualization: Puzhen Huo
Writing – original draft: Puzhen Huo
Writing – review & editing: Peng Lu, Matti Leppäranta, Georgiy Kirillin, Bin Cheng, Fei Xie, Zhijun Li

Abstract Shallow lakes (<2 m depth) of Central Asian, receiving strong solar radiation and low precipitation, are sensitive to atmospheric forcing because of their low heat capacity, yet their under-ice thermal conditions remain poorly investigated. We conducted the first complete ice season monitoring of Lake Ulansu (Ulansuhai, Wuliangsuhai), revealing unique thermal behavior. The lake was salinity stratified (<3‰), stabilizing the lower water layer and allowing the water temperature to reach 10°C before break-up. The solar radiation absorbed by the water (Q_{sw}) drove the water–ice heat flux, with approximately 82% of Q_{sw} returning to the ice base, facilitating a rapid shift from convective mixing to stable stratification. These findings provide key insights into the thermal regimes of Central Asian shallow lakes, informing climate models and ecological assessments for more than 10,000 similar lakes in the region.

Plain Language Summary We conducted the first complete ice season monitoring of Lake Ulansu (Ulansuhai, Wuliangsuhai), a shallow lake in Central Asia, using the floating remote observation system. We found that after the lake froze, the water temperature quickly rose and remained unusually warm for more than 90% of the ice season due to salinity stratification. This warming was driven primarily by intense solar radiation that penetrated the ice and was absorbed by the water body. Approximately 82% of the absorbed solar energy was transferred back to the ice base, contributing to the water–ice heat flux (F_w). The seasonal average F_w was 27.2 W m^{-2}, substantially accelerating ice melt. The lake experienced rapid and substantial heat exchange with the atmosphere before freeze-up and after break-up, highlighting the sensitivity of shallow lakes to environmental changes. These findings emphasize the major role of solar radiation in controlling the under-ice thermal regime and provide crucial insights for predicting changes in more than 10,000 similar shallow lakes in Central Asia.

1. Introduction

Globally, there are more than 250,000 water bodies with depths less than 2 m (Messager et al., 2016), 70% of which undergo seasonal cycle of freezing and melting. More than 10,000 shallow lakes are located in Central Asia (Messager et al., 2016), 98% of which experience seasonal ice cover. These shallow lakes play crucial roles in hydrological (Pi et al., 2022), carbon (Du et al., 2023; Stepanenko et al., 2016), and climate processes (Filazzola et al., 2020; Stepanenko et al., 2019). Their seasonal variations, especially in winter, alter the physical and chemical properties of lakes, such as water temperature profiles (X. Li et al., 2022), nutrient availability (Zhou et al., 2023), and dissolved oxygen levels (Ali-Maher & Bengtsson, 2020; Perga et al., 2023), thereby affecting ecosystem stability and productivity. These transformations directly impact the biological communities around lakes (Ruhland et al., 2023).

The under-ice thermal regime is key to understanding the seasonal variations in ice cover and lake water (B. Yang et al., 2017). Existing studies on under-ice physical processes have focused predominantly on Arctic and boreal lakes (Bogdanov et al., 2023; Bouffard et al., 2019; Kirillin et al., 2015), where thick snow cover limits heat sources primarily to sediment conduction (Kirillin et al., 2012; Salonen et al., 2010; Zdorovennova, 2009), maintaining the water temperature below the maximum density temperature ($T_m \approx 3.98$°C for fresh water) for extended periods (Kirchner et al., 2024; B. Yang et al., 2021). Solar radiation penetration, and consequently convective mixing within the water column, generally occurs during the late melt phase when snow cover diminishes (Klanten et al., 2024; Leppäranta et al., 2019). Similarly, studies on the Qinghai–Tibet Plateau have focused primarily on deep lakes, where high volumetric heat capacity delays warming above T_m until late melting occurs (Kirillin et al., 2021; Lazhu et al., 2021). In contrast, shallow lakes in Central Asia, characterized by strong

solar radiation and sparse snowfall, have lower volumetric heat capacities than deep lakes (Vanderkelen et al., 2020), making them more responsive to weather variations. These conditions facilitate mixing throughout the water column, possibly reaching the lake bottom (Kirillin & Shatwell, 2016), which significantly alters the under-ice thermal structure. Despite their physical regimes being distinct from those of deep lakes, the mechanisms governing under-ice heat transfer in shallow lakes remain poorly understood. This knowledge gap primarily occurs due to the inherent challenges of conducting field observations during the ice season. Safety concerns often restrict data collection to periods when the ice thickness is sufficient to support equipment and personnel, whereas instruments are typically removed before the onset of ice decay to avoid damage (Lu et al., 2020; Xie et al., 2022). Although remote sensing and numerical modeling provide alternative approaches, they often face limitations due to resolution constraints and parameter uncertainties (Su et al., 2020; Wang et al., 2022).

In this study, an innovative floating remote observation system (FROS) is employed to conduct the first comprehensive seasonal monitoring of Lake Ulansu (Ulansuhai, Wuliangsuhai). This system captures continuous meteorological data and ice–snow environmental metrics, overcoming the limitations of traditional field observations (Xie et al., 2022). Our analysis focuses on evaluating under-ice water temperature variations and the heat balance of the water column. By quantifying the primary drivers of under-ice thermal regimes, we provide novel insights into the mechanisms of heat transfer beneath ice in shallow lakes in Central Asia.

2. Study Area

Lake Ulansu (40°46′–41°7′N, 108°41′–108°58′E) is located in Inner Mongolia, China, adjacent to the Yellow River (Figure 1a). The north–south elongated lake covers 306 km^2. Approximately 40% of the lake area is open, and the remaining lake area is covered by dense reed (*Phragmites australis*) stands (G. Li et al., 2025), providing a vital habitat for various waterfowl and migratory birds. Transpiration from reeds, combined with lake evaporation, exceeds regional precipitation by more than tenfold (F. Yang et al., 2016). The lake has an average depth of 1.6 m. It relies primarily on summer inflows from the Yellow River, whereas inflow and outflow are very small during winter (Huang et al., 2022). In the last decade, Lake Ulansu has had an average annual ice duration of 4 months (Huo et al., 2022), significantly reducing air–water interactions and evaporation. Under ice-free conditions, salinity typically falls within 1.9 ± 0.6‰. As ice forms, salt exclusion and extensive freezing in this shallow lake increase under-ice salinity to 2.4–5.2‰, resulting in a stronger wintertime vertical salinity gradient compared to the ice-free season (F. Yang et al., 2016). The region experiences a temperate continental climate with cold and dry winters. Over the past 80 years, the average air temperature and wind speed have reached 7.1°C and 2.6 m s^{-1}, respectively (Huo, Lu, Cheng, et al., 2025). Situated at 1,050 m elevation, the lake receives abundant sunshine, with an average annual solar radiation of 226 W m^{-2}. The annual precipitation is 310 mm, which falls mostly in summer, and from January to March, only 6% of the total precipitation occurs.

3. Data and Methods

3.1. Field Observations

To investigate the life cycle of seasonal lake ice, we conducted observations during the 2022–2023 ice season in Lake Ulansu. The FROS was deployed on 20 November 2022, enabling continuous monitoring of under-ice physical processes until 21 March 2023. This marked the first successful collection of complete meteorological and ice-season data, capturing the entire freezing–melting cycle of the lake (Figure 1b).

The FROS collected meteorological data, including air temperature, wind speed, and incident shortwave radiation, using a compact weather station (MaxiMet GMX 501) positioned 2 m above the ice surface (see Xie et al. (2022) for technical details). Reflected shortwave radiation was measured with a TBQ-2 sensor (1 W m^{-2} accuracy) approximately 0.85 m above the ice surface. The snow depth was monitored by an SR50A ultrasonic sensor (1 cm accuracy) at the same height as the reflected shortwave radiation sensor. The temperature distributions in water, ice and sediment were monitored using 16 platinum resistance sensors (PTWD, Jinzhou Sunshine Technology, 0.1°C accuracy) with spatial resolutions of 7–25 cm. Ice thickness was measured with a Tritech PA500 ultrasonic sensor (2.5 mm accuracy) positioned 0.95 m below the ice surface.

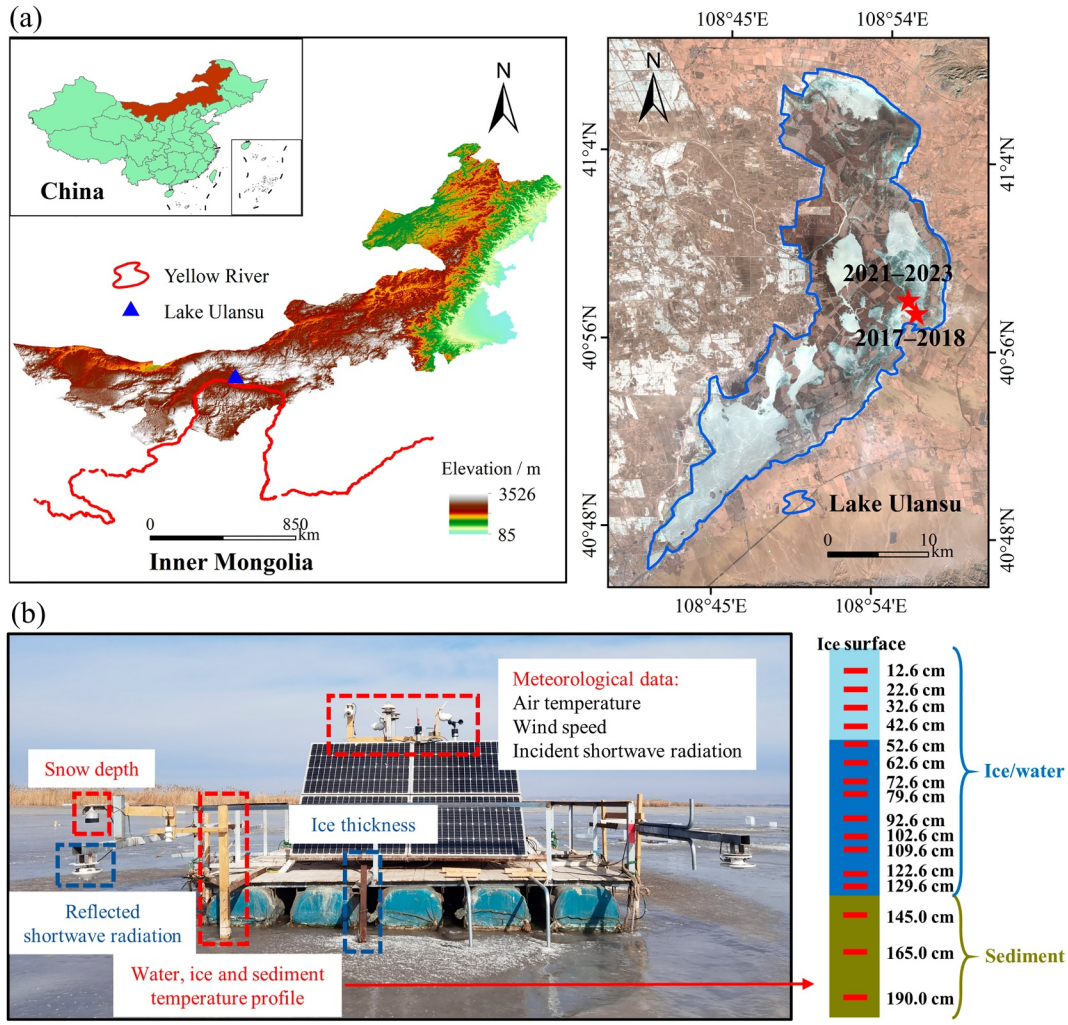

Figure 1. (a) Locations of Lake Ulansu and the experimental sites visited over 3 years (the right image is from Sentinel-2 on 1 January 2023). (b) Configuration of the floating remote observation system for field observations at Lake Ulansu in 2022–2023 ice season.

3.2. Heat Balance Beneath the Ice Cover

The heat balance at the ice–water interface expresses the water–ice heat flux F_w as the difference between the conductive heat flux F_c at the ice base and the latent heat flux due to freezing or melting F_l (Aslamov et al., 2014):

$$F_w = -F_c + F_l = -\kappa_i \frac{dT_i}{dz}\Big|_{z=h_i} + \rho_i L_f \frac{\partial h_i}{\partial t} \quad (1)$$

where κ_i is the thermal conductivity of ice, which is 2.1 W m^{-1} °C^{-1}; T_i and h_i are the temperature and thickness of the ice, respectively; ρ_i is the ice density; and L_f is the latent heat of fusion of the ice. The vertical coordinate z is defined as positive downward. The two key components F_c and F_l are derived from field observations (Figure 1b) of the ice temperature gradient ($dT_i/dz \approx \Delta T_i/\Delta z$, $\Delta z \leq 10$ cm) and changes in ice thickness ($\partial h_i/\partial t \approx \Delta h_i/\Delta t$) at the ice–water interface, respectively.

In ice-covered aquatic basins, assessing the energy distribution within the water column is pivotal for comprehending its impact on the overall heat budget. The heat balance under the ice cover is driven by the solar radiation absorbed by the water (Q_{sw}), as described by the following equation:

$$Q_{\mathrm{sw}} = -F_w + F_{\mathrm{Tw}} = -F_w + \rho_w c_w h_w \frac{\mathrm{d}T_w}{\mathrm{d}t} \quad (2)$$

where F_w is derived from Equation 1; F_{Tw} is the change in temperature of the water column; and ρ_w and c_w are the water density and specific heat, respectively. The total water depth at the location of the FROS is 1.35 m. The effective water depth (h_w) is calculated as $h_w = 1.35 - h_i$, with h_i being measured using an ultrasonic ranging sensor. T_w is the average water temperature. Changes in the water temperature ($\mathrm{d}T_w/\mathrm{d}t$) are derived from field observations. In Equation 2, two additional terms were not included: the heat conducted between the sediment and the water column ($F_{\mathrm{sed}} \approx \kappa_{\mathrm{sed}} \frac{\Delta T_{\mathrm{sed}}}{\Delta z}$, where $\kappa_{\mathrm{sed}} = 0.5\ \mathrm{W\ m^{-1}\ °C^{-1}}$, and $\Delta z = 20$ cm) and the heat flux attributable to the change in water column thickness ($F_{\mathrm{hw}} = \rho_{\mathrm{w}} c_{\mathrm{w}} \left(T_{\mathrm{w}} - T_{\mathrm{f}}\right) \frac{\mathrm{d}h_{\mathrm{w}}}{\mathrm{d}t}$, where T_f is the freezing point). These components are one order of magnitude smaller than Q_{sw} and are therefore considered negligible (Table S1 in Supporting Information S1).

To provide an independent validation of Equation 2, Q_{sw} can be estimated using the Beer–Lambert law, which accounts for the optical properties of snow, ice, and water:

$$Q_{\mathrm{sw}} = Q_s(1-\alpha)\gamma e^{-\lambda_s h_s - \lambda_i h_i}\left(1 - e^{-\lambda_w h_w}\right) \quad (3)$$

where the incident shortwave radiation (Q_s), lake surface albedo (α), and snow depth (h_s) are derived from field observations; the near-surface transmittance coefficient (γ) is 0.5 (Lu et al., 2020); and the light attenuation coefficients are 15 $\mathrm{m^{-1}}$ for snow (λ_s) and 2.1 $\mathrm{m^{-1}}$ for both ice (λ_i) and under-ice water (λ_w) (Cao et al., 2021; Huang et al., 2021, 2022).

4. Results

4.1. Complete Freezing–Melting Process of Lake Ice

From November 20 to 27, 2022, the daily average air temperature at Lake Ulansu hovered around the freezing point (Figure S1 in Supporting Information S1). On November 28, the temperature decreased to an average value of −7.4°C, while the wind speed increased to 4.3 m $\mathrm{s^{-1}}$. The ice formed on November 29 (Figure 2a), when the minimum instantaneous air temperature reached −18.1°C. The ice thickness steadily increased over the next 24 days at a rate exceeding 0.5 cm $\mathrm{d^{-1}}$ and reached 40 cm on the 28th day after freeze-up. In December, the daily average incident shortwave radiation was approximately 120 W $\mathrm{m^{-2}}$ due to the low solar elevation angle. Additionally, the albedo remained relatively low at noon at approximately 0.2. A warm period in early January resulted in a relatively stable ice thickness. However, on January 13, the air temperature sharply decreased to a minimum value of −20.0°C, and the wind speed peaked at 10.1 m $\mathrm{s^{-1}}$. Concurrently, brief snowfall lasting approximately 6 hr deposited approximately 2 cm of snow, which led to a significant increase in surface albedo to 0.76. The sustained strong winds redistributed the snow cover across the lake surface. Consequently, by January 15, the snow depth had increased to 19 cm at the FROS, and the snow cover had persisted for 16 days (Figure 2a). Despite the gradual increase in incident shortwave radiation, with instantaneous values exceeding 700 W $\mathrm{m^{-2}}$ at noon, the high snow albedo limited the solar heating of the lake. The third drop in air temperature occurred on January 22, with the season minimum reaching −26.7°C on January 24, thereby increasing the ice cover thickness to its maximum value of 49.6 cm on February 1.

The air temperature and solar radiation gradually increased later in the season, causing the ice cover to melt. On March 15, the ice melting rate reached a seasonal maximum of −4.7 cm $\mathrm{d^{-1}}$. Throughout the ice season, the average air temperature was −6.6°C, the average wind speed was 1.9 m $\mathrm{s^{-1}}$, and the cumulative incident shortwave radiation was 436.5 kWh $\mathrm{m^{-2}}$. The ice duration lasted for 113 days, with an average ice thickness of 37.5 cm.

4.2. Under-Ice Thermal Structure

Prior to ice formation, Lake Ulansu exhibited strong mixing across the entire water column due to surface cooling and wind, rendering the shallow lake responsive to atmospheric forcing. The low water salinity (approximately 1.5‰) was evenly distributed by wind-driven and convective mixing, having a minimal impact on stratification

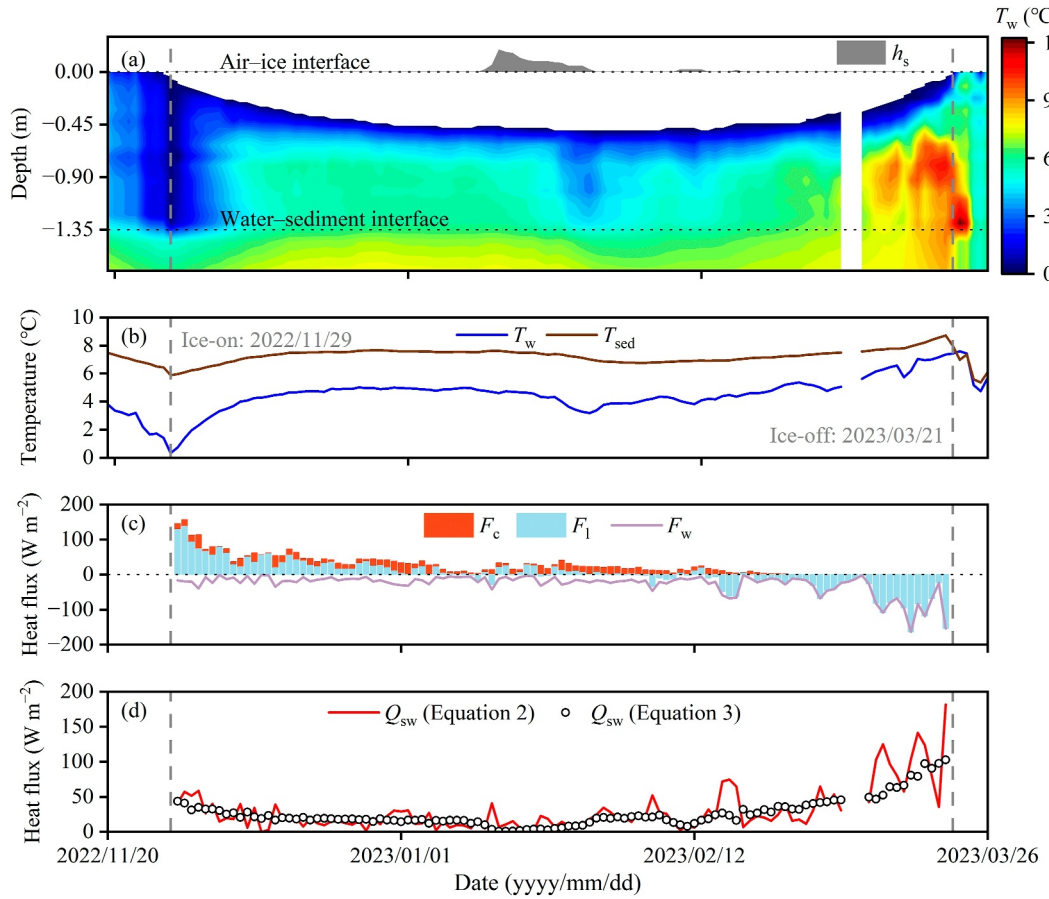

Figure 2. 2022–2023 ice season processes at Ulansu Lake. (a) Snow depth (h_s) and under-ice temperature. (b) Average water temperature (T_w) and sediment temperature (T_{sed}). (c) Conductive heat flux (F_c), latent heat flux (F_l), and water–ice heat flux (F_w). (d) Solar radiation absorbed by the water column (Q_{sw}), which is calculated via the water column heat balance method (red line) and the Beer–Lambert law (open circles).

(Guo et al., 2024; Shi et al., 2023). Over a 9-day period (Figure 2b), the average water temperature decreased from the maximum density temperature ($T_m \approx 3.76$°C) to a temperature near the freezing point ($T_f \approx -0.05$°C). During this cooling phase, the sediment temperature was higher than the water temperature and declined uniformly at a rate of approximately 0.2°C d^{-1}, indicating substantial heat transfer from the sediment to the water column, which was subsequently released to the atmosphere. The abrupt drop in air temperature to an average of −7.7°C on November 28 led to decreases in water and sediment temperatures of 1.1°C and 0.6°C, respectively, resulting in a strong heat flux of >300 W m^{-2} from the lake to the atmosphere via longwave radiation and turbulent heat losses (Table S2 in Supporting Information S1). At the start of ice cover formation the next day, the average water temperature reached 0.3°C.

Ice formation insulated the water column from the atmosphere, reducing heat loss via evaporation and longwave radiation. In turn, the newly formed thin and transparent ice permitted a substantial amount of shortwave radiation to penetrate the water column to the sediment (Figure 2d). The shallow depth of Lake Ulansu facilitated rapid increases in the water and sediment temperatures by solar radiation to the maximum density temperature within 1 week after both ice formation and thermal homogenization by free convection (Figure 2b). The bulk heating of the water column increased the downward temperature gradient in the conduction layer (CL, defined as the extent between the ice–water interface and the depth of the maximum water temperature) while reducing the CL thickness. The average water temperature exceeded T_m within 10 days following ice formation. Consequently, free convection gradually ceased, and the water column became stably stratified, with heat transfer being dominated by shortwave radiation absorption and conductive heat transport from the sediment. This transition

resulted in a stable stratified structure characterized by a CL thickness of 46.3 ± 4.5 cm and a temperature gradient within the CL of 11.9 ± 1.4°C m^{-1}.

The onset of snowfall on January 13 increased the albedo and light attenuation, reducing the amount of solar radiation absorbed by the water column (Figure 2d). Owing to heat loss through the ice cover, the temperatures of both the water and sediment decreased, although insulation by snow reduced this loss. Consequently, an increase in thickness and a reduction in the temperature gradient resulted in a CL. This process persisted until the ice surface became bare when the CL reached a maximum thickness of 80 cm (Figure 2a), corresponding to almost full-depth conduction in the water column under the ice. However, when solar radiation penetrating the ice increased, the water temperature of the lower layer rapidly rose, mitigating the effects of snowfall events.

Near the maximum ice thickness, stable ice cover led to peak salinity (2–2.5‰) in the water column (Text S1 in Supporting Information S1). This salinity induced density differences that exceeded the influence of temperature, promoting stable stratification of the water column. During the late melting stage, continuous meltwater input diluted the salinity of the upper layer, which supported the stability of stratification, while the water temperature continued to increase. The average water temperature exceeded 6°C, and the temperature difference between the water and sediment significantly narrowed. On March 9, at a depth of approximately 60 cm from the ice bottom, the temperature in the water column peaked (Figure 2a). The temperature above this peak decreased because of upward heat transfer toward the ice bottom. We hypothesized that the decrease in temperature below this peak was influenced by the vertical distribution of solar radiation absorbed within the water column and by heat absorption through the sediment. The temperature changes before break-up on March 21 further validated this assumption, showing that the shallow sediment, after absorbing solar radiation and heat from the water column, had temperatures higher than those of the bottom sediment. After the ice had completely melted, the water column and sediment of Lake Ulansu released heat to the atmosphere over three days at an average rate of >100 W m^{-2} through longwave radiation and turbulent heat losses (Table S2 in Supporting Information S1).

4.3. Heat Transfer in the Water Beneath Ice

The heat transfer at the ice–water interface F_c was considered critical for the freezing and melting of the columnar congelation ice, F_l. In December, F_l remained consistently positive (Figure 2c), with an average value of 42.3 W m^{-2} corresponding to an ice growth of 1.2 cm d^{-1} (Table S1 in Supporting Information S1). The F_c transferred the latent heat released at the interface upward through the ice and eventually released it into the atmosphere. This process was driven by the mean temperature gradient across the ice cover. The average F_c in December was 58.2 W m^{-2}. From a physical perspective, the flux from water to ice, F_w, was determined by the temperature gradient and flow within the CL beneath the ice. During the early ice growth phase, the water column was characterized by rapid solar heating accompanied by convective mixing. As a result, in December, F_w reached an average value of 15.9 W m^{-2}, which accounted for 27.3% of the heat conducted upward by F_c and released into the atmosphere. During the melting period, the ice temperature approached an isothermal state at the melting point, causing the F_c to reach zero and no heat conduction through the ice. Consequently, F_w and the F_l became balanced. In March, F_w reached 75.6 W m^{-2}, corresponding to an ice melting rate of approximately 2.2 cm d^{-1}. For the entire 2022–2023 ice season, F_w averaged 27.2 W m^{-2}, demonstrating a continuous contribution of heat transferred through the CL to decelerate ice growth/accelerate ice melt at the ice base.

The heat source in the heat balance of the under-ice water column (Equation 2), that is, Q_{sw}, balanced the heat sink F_w. Despite the lower incident solar radiation in December, the thin ice cover allowed for greater absorption of solar radiation (Figure 2d), with an average heat gain, F_{Tw}, of 5.6 W m^{-2}, which was the highest monthly average throughout the ice season. Furthermore, the temperature difference between the water column and the sediment tended to stabilize (Figure 2b), leading to a continuous decrease in the F_{sed} during the ice season, from 1.7 W m^{-2} in December to 0.2 W m^{-2} in March. Occasional snowfall events caused fluctuations in the F_{Tw} and F_w, primarily due to a reduction in the Q_{sw}. As the melting period progressed, the decrease in ice thickness was inevitably accompanied by an increase in the Q_{sw}, resulting in accelerated melting at the ice base. The average Q_{sw} and F_{Tw} values from the 2022–2023 ice season were 31.1 and 3.9 W m^{-2}, respectively.

5. Discussion

5.1. Uncertainties in Heat Flux Estimation

A comparative analysis of the results from the two methods (Equations 2 and 3) reveals a small average discrepancy of 3.6 W m^{-2} in the calculated Q_{sw} values (Figure 2d) due to methodological differences. The uncertainty of the Beer–Lambert law used in Equation 3 refers mainly to constant extinction coefficients for snow, ice, and water, which do not account for dynamic changes due to factors such as gas bubbles, colored dissolved organic matter, particles, and chlorophyll throughout the ice season (Leppäranta, 2015). In contrast, the water column heat budget approach (Equation 2) incorporates a broad range of thermal processes, including heat gain F_{Tw}, source Q_{sw} and sink F_w, allowing for a more comprehensive estimation of under-ice heat fluxes. F_w values are validated by comparing the cumulative external heat input with the observed changes in ice heat content throughout the ice season, alongside the validation of the F_c results (Text S2 in Supporting Information S1). While Equation 2 may slightly underestimate horizontal convection and diffusion, the Coriolis effect can be relevant in lakes with significant horizontal depth variations (Ramón et al., 2021; Ulloa et al., 2019). However, in the shallow Lake Ulansu, strong lateral temperature gradients are unlikely to develop, and vertical heat flux dominates over advective processes (Huang et al., 2019; Kirillin et al., 2021). Thus, this method captures the thermal variations that the Beer–Lambert law may miss, providing a more detailed representation of the under-ice heat budget.

5.2. Water–Ice Heat Flux

Assessing the F_w in an ice-covered lake is challenging, particularly in field settings where direct measurements of the internal ice temperature distribution and the ice thickness are not available. F_w depends on the temperature gradient at the ice–water interface:

$$F_w = \kappa_w \frac{dT_w}{dz}\Big|_{z=CL} \quad (4)$$

where $\kappa_w = \rho_w c_w k_w$ is the effective conductivity and k_w is the molecular diffusivity, which is 1.4×10^{-7} m s^{-2} (Bengtsson & Svensson, 1996; Shirasawa et al., 2006; Xie et al., 2023). In practice, the gradient at the interface is often replaced with the mean temperature gradient across the CL, and k_w is the effective diffusion coefficient subjected to estimation from flow properties under ice (Leppäranta, 2015; Petrov et al., 2007). Our calculations for the 2022–2023 ice season in Lake Ulansu revealed that the range of k_w was 1.6×10^{-7} to 3.3×10^{-6} m s^{-2}, with a mean value of 6.2×10^{-7} m s^{-2}, indicating substantial variability that exceeds the traditional estimate. In shallow lakes, such as Lake Ulansu, the limited depth facilitates efficient heat redistribution, leading to enhanced mixing. Unlike deeper lakes, where stratification can strongly limit mixing, shallow systems are more susceptible to dynamic thermal interactions driven by boundary fluxes. Moreover, in the presence of a bare ice surface, the thermal heterogeneity within the CL is influenced by convection driven by solar radiation. This interplay results in strong fluctuations in thermal diffusivity, as evidenced by our field observations, which static molecular diffusion coefficients cannot adequately address.

Our analysis identified solar radiation as the primary driver of F_w in Lake Ulansu. By establishing a relationship between F_w and Q_{sw} (Figure 3a), we derived the following equation:

$$F_w = 0.82\, Q_{sw} + 1.71 \quad (5)$$

Thus, 82% of the solar heat absorbed by the water column is transferred to the ice bottom. The intercept value of 1.71 W m^{-2} is suggested to arise from the heat stored in the water body. To assess the robustness of this empirical relationship, we applied it to data from the 2017–2018 and 2021–2022 ice seasons (Lu et al., 2020). The comparison between the F_w values derived from Equation 1 and those calculated using Equation 5 revealed a mean absolute error of less than 6 W m^{-2} (Figures 3b and 3c).

Building on the success of Equation 5 in Lake Ulansu, this relationship can be extended to other mid-latitude lakes in the Eurasian endorheic region, where high solar radiation in winter plays a key role, by accounting for differences in lake optical properties and water depth. An unusually high proportion of solar radiation was converted into F_w, which is a distinctive feature of shallow Central Asian lakes. For example, both Lake Ulansu and Lake

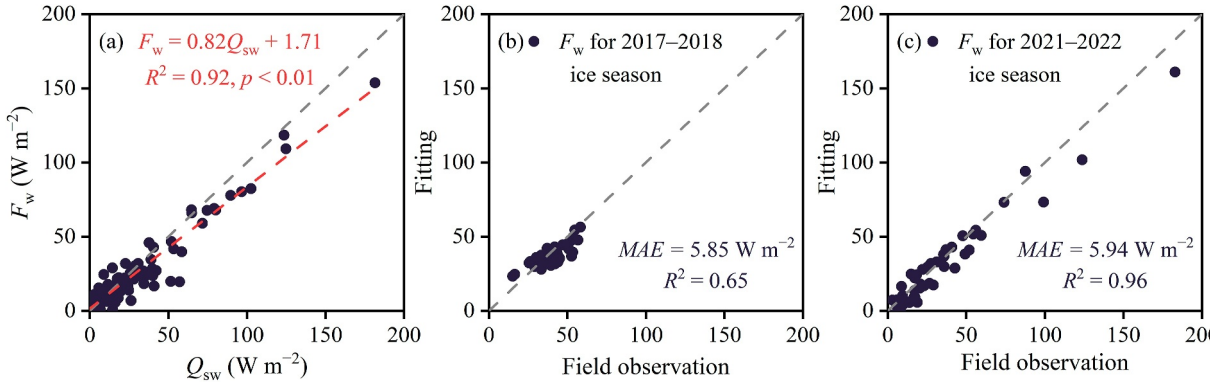

Figure 3. (a) Relationships between F_w and Q_{sw} during the 2022–2023 ice season. (b–c) Comparison of fitting and field observations for F_w during the 2017–2018 and 2021–2022 ice seasons.

BLH-A (Huang et al., 2019) exhibit rapid heating of the under-ice water following ice formation. This is driven by strong solar input, thin and patchy snow cover, and low volumetric heat capacity, which allow these lakes to reach T_m quickly, resulting in an immediate, strong, and sustained heat flux toward the ice bottom. In contrast, freshwater lakes in the North European tundra (Leppäranta et al., 2019) typically transfer only about one-third of the transmitted solar radiation to the ice bottom during the melting period, with the remaining radiation heating the water column. This discrepancy arises because, prior to the melting period, snow cover on the ice surface blocks substantial solar radiation, resulting in colder initial water temperatures. Upon snowmelt, increased solar penetration rapidly starts deepening convection in the water, reducing the proportion of radiation contributing to F_w. In turn, deep mountain lakes on the Tibetan Plateau receive comparable solar radiation during winter but have much higher volumetric heat capacity, which buffers temperature changes and delays the under-ice water temperature from exceeding T_m (Kirillin et al., 2021; Lazhu et al., 2021). According to Kirillin et al. (2021), the ratio of F_w to Q_{sw} in Tibetan lakes was 30% before the lake temperatures reach the T_m and reaches 63% afterward. Therefore, shallow lakes like Lake Ulansu, with fast thermal responses and limited heat storage, consistently exhibit a higher proportion of Q_{sw} converted into F_w.

6. Conclusion and Outlook

We presented the first complete ice season monitoring of Lake Ulansu, a large shallow, saline lake in Central Asia, using a FROS. Our observations captured unique thermal behavior within the ice–water–sediment system driven by strong solar radiation and very limited snow accumulation. As a result of strong solar radiation and salinity stratification, the average water temperature exceeded 4°C within just 10 days after freeze-up and approached 10°C before the ice break-up, significantly exceeding any previously reported values in ice-covered lakes of Northern Hemisphere. Our analysis revealed low (<2 W m^{-2}) heat conduction from sediment to water, while solar radiation absorbed by the water was the primary driver of water–ice heat flux F_w. Approximately 82% of an absorbed solar heat was returned to the ice base, producing the average F_w of 27.2 W m^{-2}, increasing to over 100 W m^{-2} in the late melting phase. The results highlighted the crucial importance of parameterizing F_w in thermodynamic models for adequate simulation of land–atmosphere interactions in cold and arid climate zones. Efficient solar energy transmission beneath ice affected thermal stability, ecosystem dynamics, and primary productivity, contributing to regional climate feedback. Future research should apply these findings to other lake systems, considering variations in optical properties and heat capacities to enhance predictive accuracy in cryospheric studies.

Data Availability Statement

The data presented in this study, including meteorological, ice, snow, and water parameters in Lake Ulansu, are available in Huo, Lu, Leppäranta, et al. (2025).

Acknowledgments
We gratefully acknowledge Editor Mathieu Morlighem and the three anonymous reviewers for their constructive comments, which significantly improved the manuscript. This work was funded by the National Natural Science Foundation of China (Grants U24A20582, 42320104004, and 42406244). GK was supported by The Federal Ministry of Education and Research of Germany (BMBF) within the framework of the Strategy "Research for Sustainability" (FONA, Sino-German collaboration project IceTMP, Project ID 01LP2006A).

References

Ali-Maher, O., & Bengtsson, L. (2020). The dependence of the consumption of dissolved oxygen on lake morphology in ice-covered lakes. *Hydrology Research*, *51*(3), 381–391. https://doi.org/10.2166/nh.2020.150

Aslamov, I. A., Kozlov, V. V., Kirillin, G. B., Mizandrontsev, I. B., Kucher, K. M., Makarov, M. M., et al. (2014). Ice–water heat exchange during ice growth in Lake Baikal. *Journal of Great Lakes Research*, *40*(3), 599–607. https://doi.org/10.1016/j.jglr.2014.06.004

Bengtsson, L., & Svensson, T. (1996). Thermal regime of ice-covered Swedish lakes: Paper presented at the 10th Northern Research Basin Symposium (Svalbard, Norway – 28 Aug./3 Sept. 1994). *Hydrology Research*, *27*(1), 39–56. https://doi.org/10.2166/nh.1996.0018

Bogdanov, S., Palshin, N., Zdorovennov, R., Efremova, T., Smirnov, S., & Zdorovennova, G. (2023). Calculation of black ice thickness and heat fluxes inside the ice and at the water–ice boundary in a boreal lake. *Limnological Review*, *23*(3), 138–156. https://doi.org/10.3390/limnolrev23030009

Bouffard, D., Zdorovennova, G., Bogdanov, S., Efremova, T., Lavanchy, S., Palshin, N., et al. (2019). Under-ice convection dynamics in a boreal lake. *Inland Waters*, *9*(2), 142–161. https://doi.org/10.1080/20442041.2018.1533356

Cao, X., Lu, P., Leppäranta, M., Arvola, L., Huotari, J., Shi, X., et al. (2021). Solar radiation transfer for an ice-covered lake in the central Asian arid climate zone. *Inland Waters*, *11*(1), 89–103. https://doi.org/10.1080/20442041.2020.1790274

Du, Y., Chen, F., Zhang, Y., He, H., Wen, S., Huang, X., et al. (2023). Human activity coupled with climate change strengthens the role of lakes as an active pipe of dissolved organic matter. *Earth's Future*, *11*(1), e2022EF003412. https://doi.org/10.1029/2022EF003412

Filazzola, A., Blagrave, K., Imrit, M. A., & Sharma, S. (2020). Climate change drives increases in extreme events for lake ice in the Northern Hemisphere. *Geophysical Research Letters*, *47*(18), e2020GL089608. https://doi.org/10.1029/2020GL089608

Guo, Y., Addo, F. G., Manirakiza, B., Zhang, T., Yin, B., Mu, X., et al. (2024). A comparative investigation of the biodiversity, assembly, and interaction of epiphytic and epipelic biofilms in shallow lakes from four geographical zones. *Process Safety and Environmental Protection*, *191*, 1956–1967. https://doi.org/10.1016/j.psep.2024.09.106

Huang, W., Zhang, Z., Li, Z., Leppäranta, M., Arvola, L., Song, S., et al. (2021). Under-ice dissolved oxygen and metabolism dynamics in a shallow lake: The critical role of ice and snow. *Water Resources Research*, *57*(5), e2020WR027990. https://doi.org/10.1029/2020WR027990

Huang, W., Zhao, W., Zhang, C., Leppäranta, M., Li, Z., Li, R., & Lin, Z. (2022). Sunlight penetration dominates the thermal regime and energetics of a shallow ice-covered lake in arid climate. *The Cryosphere*, *16*(4), 1793–1806. https://doi.org/10.5194/tc-16-1793-2022

Huang, W. F., Zhang, J. R., Leppäranta, M., Li, Z. J., Cheng, B., & Lin, Z. J. (2019). Thermal structure and water-ice heat transfer in a shallow ice-covered thermokarst lake in central Qinghai-Tibet Plateau. *Journal of Hydrology*, *578*, 124122. https://doi.org/10.1016/j.jhydrol.2019.124122

Huo, P., Lu, P., Cheng, B., Yu, M., Wang, Q., Li, X., & Li, Z. (2025). Reconstructing ice phenology of lake with complex surface cover: A case study of Lake Ulansu during 1941–2023. *The Cryosphere*, *19*(2), 849–868. https://doi.org/10.5194/tc-19-849-2025

Huo, P., Lu, P., Cheng, B., Zhang, L., Wang, Q., & Li, Z. (2022). Monitoring ice phenology in lake wetlands based on optical satellite data: A case study of Wuliangsu Lake. *Water*, *14*(20), 3307. https://doi.org/10.3390/w14203307

Huo, P., Lu, P., Leppäranta, M., Kirillin, G., Cheng, B., Xie, F., & Li, Z. (2025). Data on meteorological, ice, snow, and water parameters in Lake Ulansu [Dataset]. *Zenodo*. https://doi.org/10.5281/zenodo.15786894

Kirchner, N., Weckström, J., Jansen, J., Schenk, F., Barnett, J., Granebeck, A., et al. (2024). Water temperature, mixing, and ice phenology in the arctic–alpine Lake Darfáljávri (Lake Tarfala), northern Sweden. *Arctic, Antarctic, and Alpine Research*, *56*(1), 2287704. https://doi.org/10.1080/15230430.2023.2287704

Kirillin, G., Forrest, A., Graves, K., Fischer, A., Engelhardt, C., & Laval, B. (2015). Axisymmetric circulation driven by marginal heating in ice-covered lakes. *Geophysical Research Letters*, *42*(8), 2893–2900. https://doi.org/10.1002/2014GL062180

Kirillin, G., Leppäranta, M., Terzhevik, A., Granin, N., Bernhardt, J., Engelhardt, C., et al. (2012). Physics of seasonally ice-covered lakes: A review. *Aquatic Sciences*, *74*(4), 659–682. https://doi.org/10.1007/s00027-012-0279-y

Kirillin, G., & Shatwell, T. (2016). Generalized scaling of seasonal thermal stratification in lakes. *Earth-Science Reviews*, *161*, 179–190. https://doi.org/10.1016/j.earscirev.2016.08.008

Kirillin, G. B., Shatwell, T., & Wen, L. (2021). Ice-covered lakes of Tibetan Plateau as solar heat collectors. *Geophysical Research Letters*, *48*(18), e2021GL093429. https://doi.org/10.1029/2021GL093429

Klanten, Y., MacIntyre, S., Fitzpatrick, C., Vincent, W. F., & Antoniades, D. (2024). Regime shifts in lake oxygen and temperature in the rapidly warming High Arctic. *Geophysical Research Letters*, *51*(1), e2023GL106985. https://doi.org/10.1029/2023GL106985

Lazhu, Yang, K., Hou, J., Wang, J., Lei, Y., Zhu, L., et al. (2021). A new finding on the prevalence of rapid water warming during lake ice melting on the Tibetan Plateau. *Science Bulletin*, *66*(22), 2358–2361. https://doi.org/10.1016/j.scib.2021.07.022

Leppäranta, M. (2015). *Freezing of lakes and the evolution of their ice cover*. Springer. https://doi.org/10.1007/978-3-642-29081-7

Leppäranta, M., Lindgren, E., Wen, L., & Kirillin, G. (2019). Ice cover decay and heat balance in Lake Kilpisjärvi in Arctic tundra. *Journal of Limnology*, *78*(1). https://doi.org/10.4081/jlimnol.2019.1879

Li, G., Zhang, S., Shi, X., Zhao, S., Zhan, L., Pan, X., et al. (2025). Significant spatiotemporal pattern of nitrous oxide emission and its influencing factors from a shallow eutropic lake in Inner Mongolia, China. *Journal of Environmental Sciences*, *149*, 488–499. https://doi.org/10.1016/j.jes.2024.01.019

Li, X., Peng, S., Xi, Y., Woolway, R. I., & Liu, G. (2022). Earlier ice loss accelerates lake warming in the Northern Hemisphere. *Nature Communications*, *13*(1), 5156. https://doi.org/10.1038/s41467-022-32830-y

Lu, P., Cao, X., Li, G., Huang, W., Leppäranta, M., Arvola, L., et al. (2020). Mass and heat balance of a lake ice cover in the Central Asian arid climate zone. *Water*, *12*(10), 2888. https://doi.org/10.3390/w12102888

Messager, M. L., Lehner, B., Grill, G., Nedeva, I., & Schmitt, O. (2016). Estimating the volume and age of water stored in global lakes using a geo-statistical approach. *Nature Communications*, *7*(1), 13603. https://doi.org/10.1038/ncomms13603

Perga, M., Minaudo, C., Doda, T., Arthaud, F., Beria, H., Chmiel, H., et al. (2023). Near-bed stratification controls bottom hypoxia in ice-covered alpine lakes. *Limnology and Oceanography*, *68*(6), 1232–1246. https://doi.org/10.1002/lno.12341

Petrov, M. P., Terzhevik, A. Y., Zdorovennov, R. E., & Zdorovennova, G. E. (2007). Motion of water in an ice-covered shallow lake. *Water Resources*, *34*(2), 113–122. https://doi.org/10.1134/s0097807807020017

Pi, X., Luo, Q., Feng, L., Xu, Y., Tang, J., Liang, X., et al. (2022). Mapping global lake dynamics reveals the emerging roles of small lakes. *Nature Communications*, *13*(1), 5777. https://doi.org/10.1038/s41467-022-33239-3

Ramón, C., Ulloa, H., Doda, T., Winters, K., & Bouffard, D. (2021). Bathymetry and latitude modify lake warming under ice. *Hydrology and Earth System Sciences*, *25*(4), 1813–1825. https://doi.org/10.5194/hess-25-1813-2021

Ruhland, K. M., Evans, M., & Smol, J. P. (2023). Arctic warming drives striking twenty-first century ecosystem shifts in Great Slave Lake (Subarctic Canada), North America's deepest lake. *Proceedings of the Royal Society B: Biological Sciences*, *290*(2007), 20231252. https://doi.org/10.1098/rspb.2023.1252

Salonen, K., Shirasawa, K., Solbakov, V., Leppäranta, M., Arkhipov, B., Pulkkanen, M., & Huttula, T. (2010). Modelling circulation in an ice-covered lake. *Estonian Journal of Earth Sciences*, *59*(4), 298. https://doi.org/10.3176/earth.2010.4.06

Shi, X., Yu, H., Zhao, S., Sun, B., Liu, Y., Huo, J., et al. (2023). Impacts of environmental factors on chlorophyll-a in lakes in cold and arid regions: A 10-year study of Wuliangsuhai Lake, China. *Ecological Indicators*, *148*(1), 110133. https://doi.org/10.1016/j.ecolind.2023.110133

Shirasawa, K., Leppäranta, M., Kawamura, T., Ishikawa, M., & Takatsuka, T. (2006). Measurements and modelling of the water-ice heat flux in natural waters. In *Paper presented at proceedings of the 18th IAHR International Symposium on Ice*. Hokkaido University.

Stepanenko, V., Mammarella, I., Ojala, A., Miettinen, H., Lykosov, V., & Vesala, T. (2016). LAKE 2.0: A model for temperature, methane, carbon dioxide and oxygen dynamics in lakes. *Geoscientific Model Development*, *9*(5), 1977–2006. https://doi.org/10.5194/gmd-9-1977-2016

Stepanenko, V. M., Repina, I. A., Ganbat, G., & Davaa, G. (2019). Numerical simulation of ice cover of saline lakes. *Izvestiya - Atmospheric and Oceanic Physics*, *55*(1), 129–138. https://doi.org/10.1134/S0001433819010092

Su, D., Wen, L., Gao, X., Leppäranta, M., Song, X., Shi, Q., & Kirillin, G. (2020). Effects of the largest lake of the Tibetan Plateau on the regional climate. *Journal of Geophysical Research: Atmospheres*, *125*(1), e2020JD033396. https://doi.org/10.1029/2020JD033396

Ulloa, H., Winters, K., Wüest, A., & Bouffard, D. (2019). Differential heating drives downslope flows that accelerate mixed-layer warming in ice-covered waters. *Geophysical Research Letters*, *46*(23), 13872–13882. https://doi.org/10.1029/2019GL085258

Vanderkelen, I., van Lipzig, N. P. M., Lawrence, D. M., Droppers, B., Golub, M., Gosling, S. N., et al. (2020). Global heat uptake by inland waters. *Geophysical Research Letters*, *47*(12), e2020GL087867. https://doi.org/10.1029/2020GL087867

Wang, M., Wen, L., Li, Z., Leppäranta, M., Stepanenko, V., Zhao, Y., et al. (2022). Mechanisms and effects of under-ice warming water in Ngoring Lake of Qinghai–Tibet Plateau. *The Cryosphere*, *16*(9), 3635–3648. https://doi.org/10.5194/tc-16-3635-2022

Xie, F., Lu, P., Leppäranta, M., Cheng, B., Li, Z., Zhang, Y., et al. (2023). Heat budget of lake ice during a complete seasonal cycle in Lake Hanzhang, northeast China. *Journal of Hydrology*, *620*(1), 129461. https://doi.org/10.1016/j.jhydrol.2023.129461

Xie, F., Lu, P., Li, Z., Wang, Q., Zhang, H., & Zhang, Y. (2022). A floating remote observation system (FROS) for full seasonal lake ice evolution studies. *Cold Regions Science and Technology*, *199*(1), 103557. https://doi.org/10.1016/j.coldregions.2022.103557

Yang, B., Wells, M. G., McMeans, B. C., Dugan, H. A., Rusak, J. A., Weyhenmeyer, G. A., et al. (2021). A new thermal categorization of ice-covered lakes. *Geophysical Research Letters*, *48*(3), e2020GL091374. https://doi.org/10.1029/2020GL091374

Yang, B., Young, J., Brown, L., & Wells, M. (2017). High-frequency observations of temperature and dissolved oxygen reveal under-ice convection in a large lake. *Geophysical Research Letters*, *44*(24), 12218–12226. https://doi.org/10.1002/2017GL075373

Yang, F., Li, C., Leppäranta, M., Shi, X., Zhao, S., & Zhang, C. (2016). Notable increases in nutrient concentrations in a shallow lake during seasonal ice growth. *Water Science and Technology*, *74*(12), 2773–2783. https://doi.org/10.2166/wst.2016.433

Zdorovennova, G. E. (2009). Spatial and temporal variations of the water–sediment thermal structure in shallow ice-covered Lake Vendyurskoe (Northwestern Russia). *Aquatic Ecology*, *43*(3), 629–639. https://doi.org/10.1007/s10452-009-9277-0

Zhou, Y., Hiller, C., Andersson, S., Jakobsson, E., Zhou, L., Hawkes, J. A., et al. (2023). Selective exclusion of aromatic organic carbon during lake ice formation. *Geophysical Research Letters*, *50*(4), e2022GL101414. https://doi.org/10.1029/2022GL101414